POLITECNICO DI TORINO
Repository ISTITUZIONALE

Battery state-of-health sensitive energy management of hybrid electric vehicles: Lifetime prediction and ageing experimental validation

Original
Battery state-of-health sensitive energy management of hybrid electric vehicles: Lifetime prediction and ageing experimental validation / Anselma, P.G., Kollmeyer, P., Lempert, J., Zhao, Z., Belingardi, G., Emadi, A.. - In: APPLIED ENERGY. - ISSN 0306-2619. - 285:116440(2021), pp. 1-13. [10.1016/j.apenergy.2021.116440]

Availability:
This version is available at: 11583/2872786 since: 2021-03-01T12:53:16Z

Publisher:
Elsevier Ltd

Published
DOI:10.1016/j.apenergy.2021.116440

Terms of use:

This article is made available under terms and conditions as specified in the corresponding bibliographic description in the repository

Publisher copyright
Elsevier postprint/Author's Accepted Manuscript

© 2021. This manuscript version is made available under the CC-BY-NC-ND 4.0 license
http://creativecommons.org/licenses/by-nc-nd/4.0/.The final authenticated version is available online at:
http://dx.doi.org/10.1016/j.apenergy.2021.116440

(Article begins on next page)

16 September 2026

Battery State-of-Health Sensitive Energy Management of Hybrid Electric Vehicles: Lifetime Prediction and Ageing Experimental Validation

Pier Giuseppe Anselma,[a,b,c,*] Phillip Kollmeyer,[c] Jeremy Lempert,[c] Ziyu Zhao,[c] Giovanni Belingardi,[a,b] Ali Emadi,[c]

[a]*Department of Mechanical and Aeropsace Engineering (DIMEAS), Politecnico di Torino, 10129 Torino, Italy*

[b]*Center for Automotive Research and Sustainable Mobility (CARS), Politecnico di Torino, 10129 Torino, Italy*

[c]*McMaster Automotive Resource Centre (MARC), McMaster University, L8P 0A6 Hamilton (ON), Canada*

Elsevier use only: Received date here; revised date here; accepted date here

Highlights

- Optimal control of hybrid electric vehicles (HEVs) for fuel economy and battery lifetime
- Experimental verification of numerically predicted battery lifetime values
- Satisfactory correlation with empirical results thanks to ageing modeling update
- Significant down-sizing of HEV battery packs while preserving fuel economy

Abstract

Achieving a satisfactory high-voltage battery lifetime while preserving fuel economy is a key challenge in the design of hybrid electric vehicles (HEVs). While several battery state-of-health (SOH) sensitive control approaches for HEVs have been presented in the literature, these approaches have not typically been experimentally validated. This paper thus aims at illustrating an optimal, multi-objective battery SOH sensitive off-line HEV control approach, which is based on dynamic programming (DP) and is experimentally validated in terms of prediction capability of the battery lifetime. An experimental campaign is conducted which ages cells with current profiles for three different predicted lifetime cases. The predictive accuracy of the battery ageing model is subsequently improved by including the effect of temperature and updating the empirical ageing

* Corresponding author e-mail: pier.anselma@polito.it

characterization curve. The improved ageing model is then used to assess HEV performance in terms of fuel economy and battery lifetime for various high-voltage battery pack sizes and control goals. Results suggest that, thanks to the proposed multi-objective battery SOH sensitive control approach, the battery pack may be downsized by 35% with no impact on battery lifetime and a fuel consumption increase of just 1.1%. Engineers and designers could thus potentially adopt the proposed control approach to design HEVs which take tradeoffs between fuel economy and battery lifetime into consideration. Considerable reductions in battery pack cost, weight and production related CO2 emissions could be achieved in this way.

© 2020 Elsevier Science. All rights reserved

Keywords: battery ageing; battery state-of-health; energy management; hybrid electric vehicle (HEV); optimal control

1. Introduction

Hybrid electric vehicles (HEVs) are a key technology for achieving compliance with road vehicle tailpipe emission regulations over the next few years [1]. HEV powertrains embed different power sources which are thermal and electrical nature. Their synergetic operation is controlled by dedicated high-level energy management strategies (EMSs) [2]. These controllers perform high level management tasks including the distribution of the requested power among the components of the HEV. HEV EMSs usually aim to minimize the fuel consumption and tailpipe emissions while guaranteeing the battery state-of-charge (SOC) stays within desired limits [3]. In this framework, the impact of on-board HEV EMSs on other vehicle aspects, such as battery lifetime, is commonly disregarded from an experimental point of view. Nevertheless, several features of HEVs are deeply impacted by battery lifetime including maintenance, total cost of ownership and life cycle assessment [4]. The motivation for developing battery lifetime sensitive EMSs for HEVs can be highlighted in this framework. The ability to properly estimate the impact of the HEV powertrain operation on the high-voltage (HV) battery lifetime could indeed bring remarkable benefits both in the vehicle development phases by ameliorating the electrified powertrain sizing [5] and in the on-road operation by preventing excessive battery state-of-health (SOH) degradation [6].

Over the years many different HEV EMSs have been proposed in the literature which account for battery ageing by using numerical battery simulations. These can be divided into two categories: (1) On-line EMSs and (2) Off-line EMSs. On-line EMS’s operate in real-time and can thus find implementation in on-board HEV control units [7]. Off-line EMSs exploit the knowledge of the entire driving mission a priori to optimize the HEV powertrain operation throughout the overall journey, thus guaranteeing the optimality of the solution in terms of the control goals [8].

For on-line HEV EMSs, the equivalent consumption minimization strategy (ECMS) has most commonly been used for controlling battery ageing [9]. Ebbesen et al. first introduced a battery SOH sensitive ECMS in 2012 and applied it to a parallel HEV powertrain layout. The authors demonstrated that the proposed control approach reduced overall battery wear while limiting the impact on fuel economy, thus leading to an estimated reduction in total cost of vehicle ownership of around $4,000 [10]. In 2015, an ECMS applied to a parallel HEV with a continuously variable transmission was shown to considerably extend battery lifetime for the US06 cycle [11]. A similar EMS was recently modeled for a parallel hybrid electric city bus by Zhang et al., and savings of around 15,000 euros were predicted thanks to the usage of the same battery pack throughout the lifetime of the bus [12]. These studies show that SOH perceptive HEV EMSs may offer significant economic benefits. Further examples of on-line battery ageing sensitive EMSs are convex optimization, used by Xie et al. for a hybrid electric city bus considering real-world speed profiles [13], model-predictive control, as recently demonstrated by Cheng and Chen [14] and by Guo et al. [15], and interior point optimization, as recently proposed by De Pascali et al. [16]. Recently, a method for reducing battery capacity fade has been proposed using numerical simulations for a hybrid electric city bus that communicates with nearby vehicles to smooth vehicle speed and acceleration

Nomenclature

Acronyms

DP	Dynamic programming
ECMS	Equivalent consumption minimization strategy
EMS	Energy management strategy
HEV	Hybrid electric vehicle
HPPC	Hybrid pulse power characterization
HV	High-voltage
ICE	Internal combustion engine
MG	Motor/generator
RMS	Root-mean-square
SOC	State-of-charge
SOH	State-of-health
WLTP	Worldwide harmonized light-vehicle test procedure

Symbols

α_{batt}	Battery aging cost weighting factor
Ah_{batt}	Battery capacity
A_f	Ageing factor
Ah_{tp}	Total lifetime ampere-hour throughput
B	Pre-exponential factor
c	C-rate
δ	Tolerance on final value of battery SOC
$\Delta Ah_{batt\%}$	Percentage of battery capacity loss
i_{FD}	Final drive ratio
$i_{MG2-gear}$	MG2 reduction gearset ratio
i_{PG}	Planetary gear ratio
L_{cycle}	Drive cycle length
$Life_{batt}$	Battery kilometrical lifetime
$m_{fuel_{crank}}$	Mass of fuel required to start the ICE
$\dot{m}_{fuel}$	Rate of fuel consumption
N	Total number of battery roundtrip cycles allowed
n_P	Number of cells in parallel
P_{batt}	Battery power
R_{IN}	Battery internal resistance
SOC	Battery state-of-charge
$\dot{SOC}$	Rate of battery state-of-charge
SOH	Battery state-of-health
$\dot{SOH}$	Rate of battery state-of-health
$start_{ICE}$	ICE activation
t_0	Initial time instant
t_{end}	Final time instant
T	Battery temperature
T_{ICE}	Torque of ICE
T_{MG1}	Torque of MG1
T_{MG2}	Torque of MG2
T_{wheels}	Torque at the wheels
V_{OC}	Battery open-circuit voltage
ω_{ICE}	Angular speed of ICE
ω_{MG1}	Angular speed of MG1
ω_{MG2}	Angular speed of MG2
ω_{wheels}	Angular speed of wheels
z	Power-law factor
$\$_{batt}$	Battery cost
$\$_{fuel}$	Fuel cost

peaks, which in turn mitigate peaks in the battery power [17]. Finally, a model-predictive control strategy has been proposed and numerically studied for an HEV that considers both ageing effects and thermal effects on the battery [18].

Off-line EMSs are typically used at the development stage to determine the optimal, or best possible solution an on-line control algorithm could achieve. In one example, an off-line stochastic dynamic programming (DP) approach was formulated for a power-split HEV which accounts for anode side resistive film formation and amp-hours processed as the battery SOH metrics [19]. In another example in 2016, Patil et al. implemented a DP approach to solve a two-point optimization problem for a plug-in HEV while targeting an application-specific value of battery lifetime [20].

While several battery SOH sensitive HEV EMSs have been presented in the literature, these studies only use modeling to predict an increase in battery lifetime and do not validate these claims with experimental tests. Experimental characterization of battery ageing has been conducted for similar applications, such as start-stop vehicles [21] and mild HEVs [22], but these studies did not correlate experimental results with numerical models predicting battery capacity fading,

like those used for battery SOH sensitive EMSs. As a matter of fact, to the best of the authors' knowledge, a comprehensive experimental evaluation of the impact of HEV EMS on the battery lifetime has not yet been addressed in the literature. This paper contributes to fill the highlighted research gap by performing an experimental validation concerning the high-voltage battery lifetime predicted by a HEV EMS perceptive of the battery capacity fading. To this end, an SOH sensitive HEV EMS is first proposed in this paper, and the model predicted battery lifetime is experimentally verified for several different control cases. Subsequently, the numerical model embedded in the considered HEV EMS that predicts battery capacity fading is updated according to the results of the experimental campaign. Finally, a potential downsizing of the battery pack of a full HEV without compromising fuel economy is assessed thanks to the implemented battery SOH sensitive EMS and the updated battery ageing model.

The workflow in this paper is illustrated in Fig. 1 and involves implementing a battery ageing model, creating an SOH sensitive EMS for a power-split HEV, and then performing an experimental ageing campaign on actual battery cells for several different current profiles calculated with the proposed EMS and HEV model. The numerical battery ageing model is then updated based on the empirical results and a sensitivity study is performed on the impact of battery pack size and EMS operation on battery lifetime. The main novel contributions of this paper include (1) the development of an optimal off-line battery SOH perceptive HEV EMS based on DP, (2) a sensitivity study of the impact of the developed control approach on fuel economy and battery lifetime, (3) an experimental campaign to demonstrate the accuracy of the model predicted battery lifetime, (4) an update of the numerical model of battery ageing on the basis of the results obtained from the experiments, and (5) an evaluation of how battery pack size and EMS operation affect the predicted battery lifetime in a full HEV, with focus on downsizing the battery pack while maintaining similar fuel economy capabilities. The body of the paper is organized as follows: the numerical battery ageing model is presented in section 2, the HEV powertrain modeling and optimal control approach is given in section 3, and section 4 and 5 present the experimental tests and updated ageing model. In section 6 the battery pack size sensitivity study is performed, and finally the overall results and conclusions are discussed.

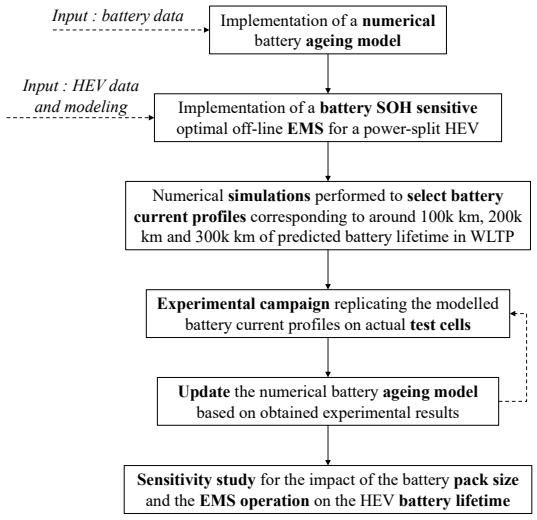

Fig. 1. Overall workflow of the paper.

2. Battery ageing modeling

The numerical approach used in this paper to model battery ageing is presented in this section. Many different ageing modeling methodologies can be found in the literature [23]. A first category includes physicochemical approaches, that can provide detailed information on the local conditions of the battery and an accurate understanding of the ageing mechanisms [24]. However, their complexity and considerable computational cost likely make them impractical to implement in on-board real-time controllers used in vehicles. A different approach uses event-oriented models, which quantify battery ageing as a function of predefined events and neglect their order of occurrence over time [25]. While this is a computationally efficient method, it necessitates a time consuming heuristic tuning processes and lacks flexibility since the battery ageing process is related to a few predefined events. Another category of ageing models includes weighted ampere-hour (Ah) models, which assume that a battery can achieve an overall

lifetime Ah throughput, which is typically weighted based on current magnitude, temperature, and other factors. These models are computationally efficient and easily adaptable to different battery technologies. Moreover, they allow the optimization of battery operating conditions, which is a fundamental requirement for implementation in HEV EMSs. As a minor drawback, they do not relate to the physical or chemical properties of the cell, rather they rely mostly on the statistical interpretation of experimental data. Thanks to its effectiveness, an Ah model from [10] is implemented in this paper to estimate battery ageing.

The SOH of a battery at a generic time instant t_i can range from 1 (beginning of life) to 0 (end of life) and is defined as follows:

$$SOH(t_i) = SOH_0 - \int_0^{t_i} \dot{SOH}(c,T)\, dt$$
$$\text{with } \dot{SOH}(c,T) = 0.2\, \frac{c}{3600 \cdot N(c,T)} \quad (1)$$

where SOH_0 is the initial SOH, $\dot{SOH}$ is the reduction in SOH at each time step, c denotes the instantaneous battery C-rate calculated as the ratio between the current in amps and the rated battery capacity in amp-hours, and N is the number of calculated roundtrip cycles before the battery reaches its end-of-life. The factor of 0.2 is to account for the factor N being calculated for a 20% reduction in residual capacity which is synonymous with SOH. The factor of 3600 is to covert the units of c from 1/h to 1/s. N is not a constant value, it is a function of the battery operating conditions (i.e. C-rate and temperature T). In order to determine N, the percentage of battery capacity loss $\Delta Ah_{batt\%}$ needs to be evaluated according to the approach proposed by Bloom et al. in 2001 [26]. This takes inspiration from the Arrhenius equation which describes the behavior of ideal gases. However, the general equation has been edited as follows to apply it to battery ageing [27]:

$$\Delta Ah_{batt\%} = B(c) \cdot e^{-\frac{A_f(c)}{T}} \cdot {Ah_{tp}}^{z} \quad (2)$$

Following (2), $\Delta Ah_{batt\%}$ depends on an empirical pre-exponential factor B, the ageing factor A_f, the lumped cell temperature T, a power-law factor z and the total lifetime ampere-hour throughput Ah_{tp}. B and A_f depend on the instantaneous battery c-rate c. The numerical values for parameters of an A123 26650 $LiFePO_4$ chemistry cell are obtained from [10], where the authors declared that the numerical model parameters were determined from data published in [28]. Table 1 reports the ageing parameter values utilized. For the initial ageing modeling, the lumped cell temperature is assumed to be a constant value of 25°C.

Table 1

Battery Ageing Parameters for a A123 26650 cell

Parameter	Value	Units of measure
Ageing factor, A_f	3,814.7 – 44.6·c	K
Power law factor, z	0.55	-
Temperature, T	298	K
Empirical pre-exponential factor $B(c)$	[21,681 ; 12,934 ; 15,512 ; 15,512]	-
Current C-rate, c	[2; 6; 10; 20]	-

For determining how many cycles the HEV battery can provide, it is assumed that end of life corresponds to a loss of 20% of initial capacity, so a value of 20% is used for $\Delta Ah_{batt\%}$. By using this value and solving (2) for $Ah_{tp}(c)$, the total number of lifetime roundtrip cycles N can be calculated as a function of c-rate in (3),

$$N(c,T) = \frac{Ah_{tp}(c,T)}{2 \cdot Ah_{batt}} \quad (3)$$

where Ah_{batt} is the rated battery capacity in ampere-hours (i.e. 2.5 Ah for the A123 cell). The factor of two in the denominator is to account for Ah_{tp} including both the charge and discharge Ah. Fig. 2 illustrates the number of allowed battery roundtrip cycles for different temperatures as given by the implemented ageing model. The experimental data from [28] includes ageing results up to a c-rate of 10. However,

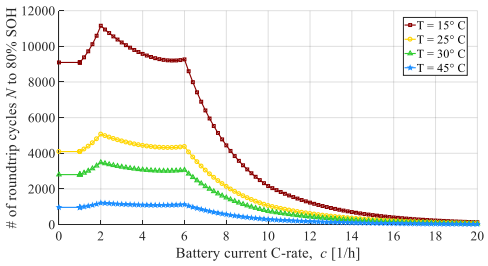

Fig. 2. Number of allowed battery roundtrip cycles as function of the C-rate as predicted by the implemented ageing model.

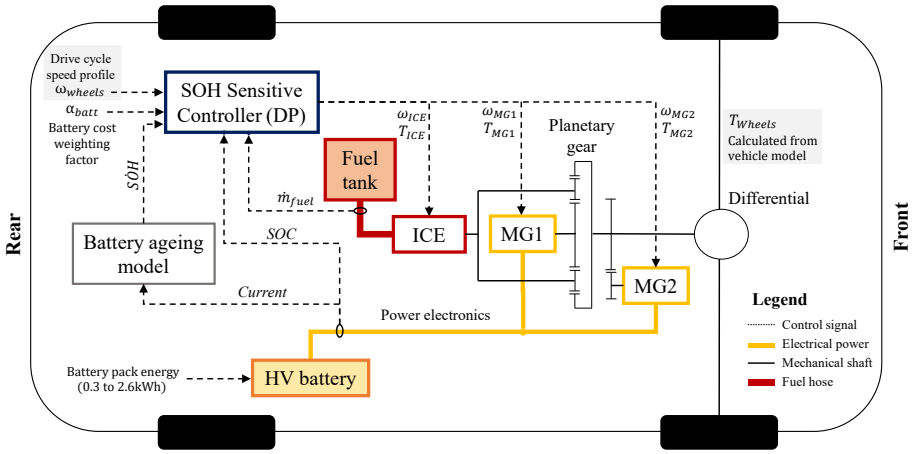

Fig. 3. Schematic diagram of SOH sensitive control algorithm implementation with modelled HEV drivetrain

since this value might likely be exceeded in some cases of HV battery operation in real-world driving of HEVs, an extension of the ageing model up to C-rate values of 20 has been initially performed by retaining the same value of B after the C-rate value of 10 in Fig. 2.

Predicting the residual battery lifetime is thus possible using the described model. For the modeling in this paper, it is assumed that all the cells of the battery pack are identical and that they exhibit the same state conditions such as SOC and SOH. The battery ageing model also assumes that ageing is independent of SOC, an assumption supported by the ageing tests in [28]. This also is likely the case for this application because the HEV powertrain is controlled to operate in charge sustaining mode, where the battery SOC stays within a narrow band.

3. HEV powertrain modeling and battery state of health sensitive optimal control

The HEV powertrain layout considered in this study is described in this section, along with related modeling and the proposed optimal control approach. An overview of the concept is provided in Fig. 3 and described as follows. The dynamic programming (DP) based battery SOH sensitive controller is responsible for commanding the internal combustion engine and two motor generators (MG1 and MG2) to create the torque at the wheels to follow the drive cycle speed profile of interest. The controller has two optimization goals: (1) to minimize fuel consumption, $\dot{m}_{fuel}$, and (2) to minimize the reduction in battery state of health, $\dot{SOH}$, or in other words to maximize battery lifetime. The battery cost weighting factor α_{batt} determines how much battery lifetime is valued compared to fuel consumption. In later analysis, the fuel consumption and battery pack lifetime are analyzed as a function of α_{batt} and the battery pack stored energy, both shown in Fig. 3. The remainder of this section discusses the powertrain layout, modeling, and multi-objective optimal control design.

3.1. Electrified powertrain layout

The electrified powertrain layout used in this study is of the power-split type, as shown in the schematic diagram in Fig. 3. It features an internal combustion engine (ICE) and two electric motor/generators (MGs) which are linked to the HV battery. MG2 is the main traction motor and is directly coupled to the driven wheels through a reduction gearset. The other traction motor, MG1, the ICE and differential input shaft are respectively linked to the sun gear, ring gear, and carrier of a planetary gear set. Vehicle and powertrain data for the modeled HEV is listed in Table 2. The modeled HV battery pack is composed of A123 ANR26650M1-B cells, where the number of cells is

varied to allow the consideration of different size packs.

Table 2
Parameters of the modeled HEV

Component	Parameter	Value
Vehicle	Mass	1531 kg
ICE	Capacity	1.8 L
	Power max	72 kW @ 5,000 rpm
	Torque max	142 Nm @ 4,000 rpm
MG1	Power max	42 kW
MG2	Power max	65 kW
Transmission ratios	i_{PG} (Ring / Sun)	2.6
	$i_{MG2\text{-}gear}$	1.26
	i_{FD}	3.27
Auxiliaries	Electrical subsystem power	500 W
HV battery pack	Cell type & capacity	A123 ANR26650M1-B, 2.5Ah

3.2. HEV modeling

The electrified powertrain is modeled using a backward quasi-static approach for computing the requested speed and power values of components directly from the driving mission speed and acceleration requirements [29]. As it can be noticed from Fig. 3, the MG2 angular speed ω_{MG2} is proportionally linked to the angular speed of the driven wheels ω_{wheels}, while the MG1 angular speed ω_{MG1} depends on the ICE speed ω_{ICE} as well due to the kinematic constraints of the planetary gear set. The resulting kinematic constraints for the electrified drivetrain are therefore as follows:

$$\begin{bmatrix}\omega_{MG1}\\ \omega_{MG2}\end{bmatrix} = \begin{bmatrix}-i_{FD}\cdot i_{PG} & i_{PG}+1\\ i_{FD}\cdot i_{MG2-gear} & 0\end{bmatrix}\begin{bmatrix}\omega_{wheels}\\ \omega_{ICE}\end{bmatrix} \quad (5)$$

where i_{FD}, $i_{MG2-gear}$ and i_{PG} respectively represent the final drive or differential ratio, the MG2 reduction gearset ratio and the planetary gear set ratio. Based on the torque ratios for standard epicyclic gearing, and assuming unitary efficiency for the transmission system, torque values for both MG1 (T_{MG1}) and MG2 (T_{MG2}) can be evaluated depending on the torque request coming from road and driver (T_{wheels}) and the torque of the ICE (T_{ICE}), which is used as the control variable in (6).

$$\begin{bmatrix}T_{MG1}\\ T_{MG2}\end{bmatrix} = \begin{bmatrix}0 & -\frac{1}{i_{PG}+1}\\ \frac{1}{i_{MG2-gear}\cdot i_{FD}} & -\left(\frac{i_{PG}}{i_{PG}+1}\right)\cdot\left(\frac{1}{i_{MG2-gear}}\right)\end{bmatrix}\begin{bmatrix}T_{wheels}\\ T_{ICE}\end{bmatrix} \quad (6)$$

For the electrical energy path, the amount of power that the battery is required to either deliver or absorb (P_{batt}) is calculated as:

$$P_{batt} = \left(\sum_{i=1}^{2}\frac{P_{MGi}}{[\eta_{MGi}(\omega_{MGi},T_{MGi})]^{sign(P_{MGi})}}\right) + P_{aux} \quad (7)$$

where P_{MG} and η_{MG} respectively represent the mechanical power and the overall efficiency of an MG, which is determined from empirical lookup tables with torque and speed as independent variables [30]. The sign of P_{MG} is utilized as an exponent in the denominator to properly account for efficiency in motoring or generating cases. Finally, P_{aux} is the power consumed by the accessories (e.g. lighting, air conditioning) and is assumed having a constant value here. The variation in battery SOC for a timestep is then determined by calculating battery current with an equivalent open circuit model as in (8) and assuming a time step of one second:

$$\dot{SOC} = \frac{V_{OC}(SOC)-\sqrt{[V_{OC}(SOC)]^2-4\cdot R_{IN}(SOC)\cdot P_{batt}}}{2\cdot R_{IN}(SOC)}\cdot\frac{n_P}{Ah_{batt}\cdot 3600} \quad (8)$$

where R_{IN} is the internal resistance and V_{OC} is the open circuit voltage of the full battery pack, as obtained from SOC dependent lookup table that can be determined from data in the cell manufacturer catalogue [31]. n_P is the number of cells in parallel for the given battery pack configuration and Ah_{batt} is the rated Ah for a single cell as defined earlier.

For the ICE, the instantaneous rate of fuel consumption $\dot{m}_{fuel}$ and the corresponding efficiency are determined with an experimental steady-state lookup table with speed and torque as independent variables [32].

3.3. HEV battery state of health sensitive multi-objective optimal control

Dynamic programming, a widely adopted tool which can be used for off-line optimal control of an HEV [33], is implemented here. This algorithm finds the global optimal solution for a control problem by exhaustively searching through all possible discretized

values of state and control variables [34]. For the implementation here, the DP algorithm is configured to minimize the overall value of the cost function J for the entire driving mission under analysis:

$$\begin{gathered} J = \int_{t_0}^{t_{end}} \{ [\dot{m}_{fuel} + m_{fuel_{crank}} \cdot (start_{ICE} > 0)] \cdot \$_{fuel} \\ + \alpha_{batt} \cdot \$_{batt} \cdot \dot{SOH} \} \, dt \\ \text{subject to:} \\ SOC(t_0) \leq SOC(t_{end}) \leq SOC(t_0) + \delta \\ \omega_{ICE_{min}} \leq \omega_{ICE} \leq \omega_{ICE_{MAX}} \\ \omega_{MG1_{min}} \leq \omega_{MG1} \leq \omega_{MG1_{MAX}} \\ \omega_{MG2_{min}} \leq \omega_{MG2} \leq \omega_{MG2_{MAX}} \\ 0 \leq T_{ICE} \leq T_{ICE_{MAX}}(\omega_{ICE}) \\ T_{MG1_{min}}(\omega_{MG1}) \leq T_{MG1} \leq T_{MG1_{MAX}}(\omega_{MG1}) \\ T_{MG2_{min}}(\omega_{MG2}) \leq T_{MG2} \leq T_{MG2_{MAX}}(\omega_{MG2}) \\ SOC_{min} \leq SOC \leq SOC_{MAX} \\ c \leq c_{MAX} \end{gathered} \tag{9}$$

where $\dot{m}_{fuel}$ and $m_{fuel_{crank}}$ are the fuel rate consumed by the ICE at each time instant (as computed following the HEV model described in section 2.3) and the fuel mass required to start the ICE, respectively. $m_{fuel_{crank}}$ represents a constant quantity here and its value is set to 1 gram being contained in the suitable range indicated for a 4-cylinder gasoline ICE in [35]. The parameter $start_{ICE}$ is a binary variable which indicates an ICE activation occurrence. The variables $\$_{fuel}$ and $\$_{batt}$ denote cost values respectively for fuel and for the battery. $\$_{fuel}$ is based on the June 2020 averaged US gasoline price of 2.25 $/gallon [36], while a value of $3,000 is used for $\$_{batt}$ from [37]. $\dot{SOH}$ is the instantaneous rate of battery SOH as evaluated using the numerical ageing model described in section 2, while α_{batt} is a scaling coefficient which tunes the cost of the battery. The higher the α_{batt} value, the more value is placed on the battery, resulting in a reduction of battery ageing at the expense of fuel economy. When solving the optimal control problem, the battery SOC is set to have similar values at the beginning and end of the considered driving missions assuming an appropriate tolerance δ, guaranteeing that charge is sustained. Finally, both battery SOC, battery C-rate and the torque and speed of power components are constrained within the corresponding allowed operating regions.

The power-split HEV has two operating modes, pure electric or hybrid. During pure electric operation, the HV battery supplies or absorbs power from MG2, which is the only active source of power to the wheels. In hybrid mode all of the power components – MG1, MG2, and the ICE – are active. The speed and torque of the ICE is controlled by the EMS, while MG1 is mainly used to allow the ICE speed to be independent of wheel speed and to generate electrical energy. The HEV operation is managed with the following control variable set U containing speed and torque values for the ICE as formulated in (10).

$$U = \begin{Bmatrix} \omega_{ICE} \\ T_{ICE} \end{Bmatrix} \tag{10}$$

Pure electric operation corresponds to a value of 0 for both ω_{ICE} and T_{ICE}. These two control variables are sufficient for establishing the operating conditions of all the remaining power components of the hybrid electric powertrain. The DP states are, by definition, the parameters which depend on the preceding time steps, and consist of X for this system:

$$X = \begin{Bmatrix} SOC \\ ICE_{on/off} \end{Bmatrix} \tag{11}$$

where battery SOC represents a state as it is the integral of the battery current and the ICE state (i.e. on/off) is considered because each cranking event consumes a specified amount of fuel and cranking events are only allowed at a certain frequency (around once every 110 seconds) so the comfort of the ride is reasonable.

4. Design of three battery lifetime cases and experimental campaign

This section describes the development of test cases which vary the battery pack size and control function to achieve three different predicted battery lifetimes. The experimental test procedure and the setup utilized for the selected tests is also described.

4.1. Selection of test cases

The multi-objective HEV optimal control algorithm presented in section 3.3 can be used to size the battery pack and tune the controller to achieve both good fuel economy and a reasonable lifetime for the battery

pack. To demonstrate this, a range of test cases are modeled, with battery pack size varying from 0.3 kWh to 2.0 kWh, and battery aging cost weighting coefficient $\boldsymbol{\alpha_{batt}}$ varied from 0.0 to 0.2. For the prediction of battery aging, the worldwide harmonized light-vehicle test procedure (WLTP) is considered to repeat continuously for the life of the vehicle. The predicted lifetime in kilometers $\boldsymbol{Life_{batt}}$ is calculated following (12):

$$Life_{batt} = 0.2 \cdot \frac{L_{cycle}}{SOH_{t_0} - SOH_{t_{end}}} \tag{12}$$

where L_{cycle} is the spatial distance in kilometers driven for the considered drive cycle, and SOH_{t_0} and $SOH_{t_{end}}$ are the values of battery SOH at the beginning and at the end of the drive cycle, respectively. The factor of 0.2 is to account for 80% SOH being considered end of life. SOH is calculated using the numerical ageing model illustrated in Section 2 and following (1) to (3).

The modeled battery lifetime and vehicle fuel consumption for the considered cases is plotted in Fig. 4. With a larger battery pack, peak current in the battery is smaller, resulting in a longer lifetime. Larger packs are also able to provide more power and energy resulting in reduced fuel consumption. When α_{batt} is 0, the DP controller only considers fuel consumption, and as α_{batt} is increased the controller values battery lifetime more, resulting in as much as five times greater battery life at the expense of increased fuel consumption as it can be seen in Fig. 4.

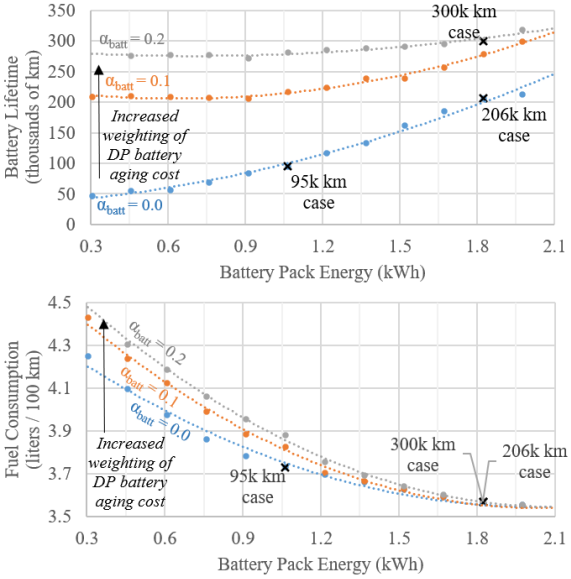

Fig. 4. Simulated WLTP drive cycle fuel consumption and predicted battery lifetime as a function of the battery pack capacity and battery aging cost weighting coefficient α_{batt}

The goal of the experimental testing is to prove the accuracy of the model predicted battery lifetime. Three cases are selected to demonstrate both dimensions of the model – lifetime as a function of battery pack size, and lifetime as a function of the aging cost weighting coefficient α_{batt}. The three selected cases, namely the '95k', '206k', and '300k' km battery lifetime cases, are highlighted in Fig. 4. The '95k' and '206k' cases both have α_{batt} = 0 and have 1.06 and 1.82 kWh battery pack sizes respectively. The '206k' and '300k' cases both have 1.82 kWh battery packs and have α_{batt} = 0 and α_{batt} = 0.2 respectively.

The modeled current and SOC for a single battery cell from the pack for each test case is plotted in Fig. 5, showing that as predicted battery lifetime goes up battery current and SOC deviation decrease. Table 3 also shows that as predicted battery lifetime increases there is a considerable decrease in the root-mean-square (RMS) current, from 10.36 to 6.19A, and in the Ah throughput, from 1.91 to 1.10Ah. It can also be observed in Fig. 5 that a battery charging current limit of 20A was implemented in the control algorithm. This is necessary because predicted battery lifetime is calculated assuming the battery can always supply the commanded current. The charging current limit

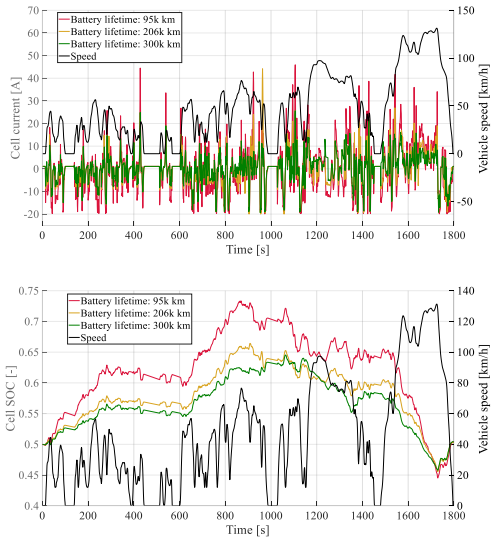

Fig. 5. Battery cell current and SOC profiles for WLTP drive cycle for each experimental test case.

Table 3

Statistics for the experimental test cases selected in WLTP

Test name	95k	206k	300k
Number of battery pack cells	140	240	240
Battery pack capacity [kWh]	1.06	1.82	1.82
Estimated fuel economy [l/100 km]	3.73	3.57	3.57
α_{batt}	0	0	0.2
Estimated battery lifetime [km * 10^3]	95	206	300
Estimated number of WLTP cycles	4,086	8,860	12,903
Current RMS [A]	10.36	7.31	6.19
Ah throughput [Ah]	1.91	1.30	1.10
Max charging current [A]	-19.9	-20.0	-19.4
Max discharging current [A]	45.9	44.2	25.6

ensures that the battery will not hit the upper voltage limit of 3.6V, resulting in the actual current being less than the commanded value.

Additional results for a wide range of battery pack sizes are also presented in the final section of the paper to give greater insight into how the control algorithm can be used to tune battery lifetime.

4.2. Battery characterization and ageing test procedure

The main goal of the experimental tests is to determine the actual battery lifetime of the cells for continued repetition of the WLTP current profiles shown in Fig. 5. The tests are conducted in a thermal chamber set to 25°C (the same value of temperature used in the numerical modelling), and the current, terminal voltage and temperature of each cell is recorded.

The testing is grouped into two sections, characterization tests and 300 WLTP ageing cycles, which are repeated until the battery SOH has fallen to at least 80%. The characterization tests consist of a 1C rate discharge capacity test and a hybrid pulse power characterization (HPPC) test, as listed in step I of Table 4. The HPPC test results are used to calculate discharge resistance versus SOC for a 10 second 1C current pulse. In step II the cell is fully charged and then discharged to 50% SOC, which is defined as 50% of the 1C capacity measured in step I. Basing the amp-hours discharged on the measured capacity ensures that as the cell ages the WLTP cycles are always performed around the midpoint of cell capacity. For Step III sixty WLTP cycles are performed, and charge is adjusted back to 50% SOC following each cycle as needed. Steps II and III are then repeated five times, for a total of 300 WLTP cycles, and all the steps are repeated until capacity fades to at least 80% of the initial value. The experimental setup will be described in the following sub-section.

4.3. Experimental test setup

The experimental tests were performed on three A123 ANR26650M1-B cells, with one of the three current profiles defined in Fig. 5 applied to each cell during the WLTP cycle portion of the ageing tests. The cells were placed in a thermal chamber and connected to a battery cycler, as shown in Fig. 6 and Fig. 7. Cell voltage is measured at the battery terminals via the battery cycler and a temperature sensor was fixed to the front center face of the cell, as is visible in Fig. 6. A +/-75A, 0-5V rated channel of an MCT 75-0/5-8ME Digatron Power Electronics battery cycler illustrated in Fig. 7(b) was used to test each cell. The voltage and current measurement and control accuracy of the battery cycler is +/- 0.1% of full scale and the accuracy of the temperature sensor is +/- 0.5°C. The cycler can regulate voltage from 0-5V, current from -75 to +75A, and power from -375 to +375W. The battery cycler utilizes an automated software, Battery Manager, which is provided by Digatron, runs on a desktop computer, and can be used to create test programs consisting of hundreds of steps and to save the results in a database. Each program step can be a pause, constant voltage, constant current, or constant power step, or a power or current profile as is used for the WLTP cycles in this test.

The battery cells were tested at a fixed temperature of 25°C in a 16 cubic foot Envirotronics SH16C thermal chamber shown in Fig. 7(a). The chamber is rated to regulate temperature to within +/- 0.3°C of the setpoint, which can vary from -68 to 177°C. The chamber can also provide 1400W of cooling power and cool at a rate of about 5°C per minute, although this is not relevant for these constant temperature tests. The testing was performed continuously on this equipment for a period of more than nine months.

Table 4

Battery cell ageing test plan

Test step	Description
I	Characterize cells: *HPPC and two repeated 1C discharge capacity tests*
II	Fully charge and then discharge to 50% SOC: *Amp-hours discharged to attain 50% SOC is based on cell capacity measured in step I*
III	Perform 20 WLTP cycles: *Adjust charge to 50% SOC following each WLTP cycle using measured Amp-hours*
IV	Repeat steps II and III 14 additional times: *For a total of 300 WLTP cycles*
V	Return to step I: *Repeat test sequence until battery capacity fades to 80% of its initial value or until time available for testing is exceeded*

Fig. 6. Tested cells mounted in the thermal chamber.

(a) Envirotronics SH16C thermal chamber *(b) Digatron MCT 75-0/5-8ME battery cell cycler*

Fig. 7. Battery test equipment for ageing test

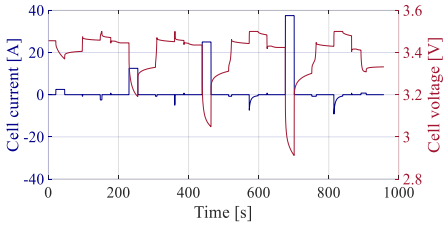

(a) HPPC test

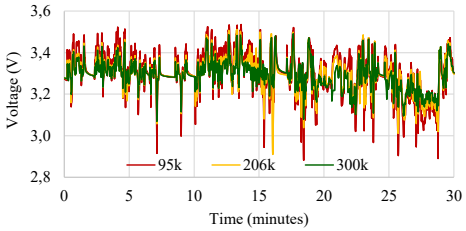

(b) WLTP cycle for each test case

Fig. 8. Experimental measurements for ‘95k’ test case.

5. Experimental results and updated empirical ageing model

The experimental results obtained from the ageing tests are presented in this section. A summary of the results for the three test cases are first presented. Then, an updated version of the numerical ageing model is created based on the empirical outcomes.

5.1. Summary ageing test results for all cells

As it has been highlighted in section 4, each group of 300 WLTP cycles is preceded by an HPPC test, a 1C discharge capacity test and a discharge to 50% SOC. Fig. 8 illustrates examples of time series results for HPPC and one of the WLTP tests. For the HPPC test, as shown in Fig. 8(a), a series of current pulses are applied to the cell at different states of charge and the cell resistance is calculated from the voltage response. For the 1C discharge capacity test, the cell starts fully charged and is discharged at a 1C (2.5A) rate until voltage reaches 2.5V. The cell is then recharged and discharged to half of the measured 1C discharge capacity (50% SOC), and the series of WLTP cycles is started. The voltage for one full WLTP cycle for each test case is given in Fig. 8(b), showing that there is significant more voltage deviation for the more aggressive, shorter lifetime test cases.

Seven to eight days were typically necessary to perform the characterization tests along with each group of 300 WLTP cycles, which sum up to around 8,000 km of driving. Since the predicted values of cell lifetime ranged from around 4,000 to around 13,000 WLTP cycles, this translated into a total testing time ranging from around 106 days to around 303 days as it has been illustrated in Fig. 9. Each of the cell tests were initiated simultaneously, but due to test equipment issues there were occasional delays which were deemed to have a minimal effect on the results. Both the 95k and 206k test cases were kept running even after the cell residual capacity felt below 80% of its initial value, thus reaching its nominal end of lifetime.

To demonstrate how the battery characteristics vary as the ageing test progresses, the 1C discharge voltage and the resistance calculated from the HPPC test are shown for each characterization test in Fig. 10 and Fig. 11. A progressive shift towards left can be observed for both the 1C discharge voltage and the resistance curves as the cells age, capacity reduces, and resistance increases. As predicted by the numerical ageing model, the 95k test case in Fig. 10(a) and Fig. 11(a) ages much more quickly than the other test cases.

The measured 1C capacity versus distance driven is given in Fig. 12(a) for both numerical and experimental results, showing that the 95k case had lifetime similar to that expected, while the 206k and

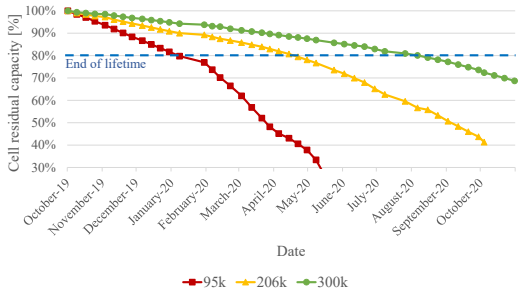

Fig. 9. Trend of residual capacity over time for tested cells.

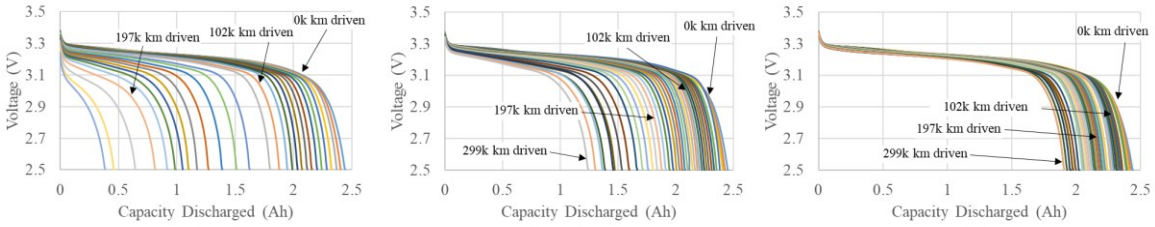

(b) 95k test case (b) 206k test case (c) 300k test case

Fig. 10. Voltage for 1C rate discharge versus km driven by the cells for the WLTP cycle

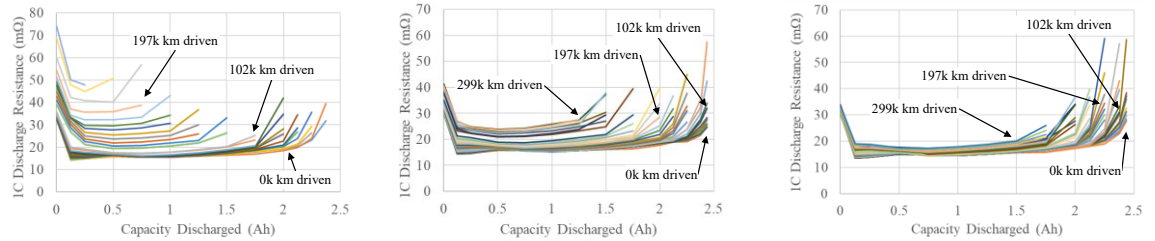

(b) 95k test case (b) 206k test case (c) 300k test case

Fig. 11. Internal 1C rate discharge resistance versus amp-hours as a function of number of km driven by the cells in WLTP.

300k cases aged somewhat more quickly than predicted by the model. Capacity is plotted in Fig. 12(b) versus the equivalent number of roundtrip cycles (i.e. lifetime Ah throughput divided by twice the rated capacity), showing that the ageing is more than just a function of number of cycles. Finally, Fig. 12(c) shows that cell resistance is relatively constant until capacity falls below 80% SOH.

The differences between the model predicted and experimental ageing results are highlighted in Table 5. The numerical prediction correlates very well with the 95k case experimental data, with an error of just 1.6% or 1000km. For the other two cases the model significantly underestimates the capacity fade though, with the cells reaching end of life earlier than expected. The empirically observed number of cycles before end of life were around 14% and 11% less than predicted for the 206k and 300k respectively. To overcome this drawback, several methods to improve the numerical ageing model are investigated in the next section.

5.2. Updating of numerical ageing model

While the ageing model does correlate fairly well with the experimental measurements, there are several significant factors which likely contributed to the mismatch between modeled and measured results:

1. The model is based off data for A123 ANR26650M1 cells (rated capacity: 2.2 Ah) [28], whereas the tested cells are a newer model, A123 ANR26650M1-B (rated capacity: 2.5 Ah). It was assumed the new cell ages identically, in terms of cycles, as the older cell.
2. The model only accounts for cyclic ageing and does not explicitly consider calendar ageing. Since the 206k and 300k tests are of longer duration, calendar ageing may result in more ageing than is predicted for these cases.
3. Battery temperature is assumed to be 25°C, but actual battery temperature is a couple degrees higher due to losses in the cell, reducing the lifetime of the cell.

Table 5

Comparison between numerical predictions and experimental results for lifetime of all tested cells

Test case	Predicted cell lifetime [km*10^3]	Experimental cell lifetime [km*10^3]	Difference [%]
'95k'	95	94	-1.6%
'206k'	206	177	-14.1%
'300k'	300	268	-10.7%

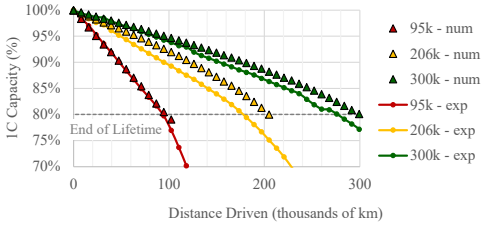

(a) Capacity versus distance driven

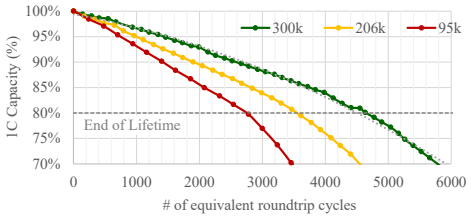

(b) Capacity versus # of roundtrip cycles

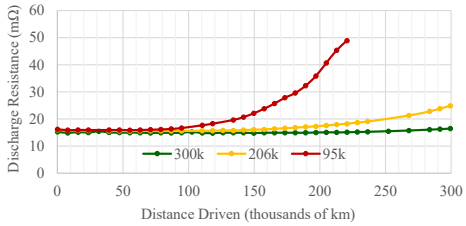

(c) 50% SOC resistance versus distance driven

Fig. 12 Battery capacity fade and resistance increase with ageing

4. The ageing model calculations neglected to include the characterization cycles, which account for 10.5 additional roundtrip cycles per 300 WLTP repetitions, causing slightly more ageing than that predicted by the model.
5. The 10C rate model parameters were used up to a 20C rate. The battery may age more quickly or more slowly beyond 10C than is calculated by this extrapolation of the test data

While data is not available to account for the first two factors listed above, the modeling methodology can be adjusted in consideration of items three, four, and five. In the next subsection, the actual cell temperature and the extra characterization cycles will be included in the model, and in the following subsection the shape of the ageing curve beyond 10C will be adjusted to achieve a better match between the modeled and measured results.

5.2.1 Accounting for temperature and extra-characterization cycles

Of all the factors influencing cell ageing which are mentioned in the previous section, cell surface temperature, which is well known to have a major impact on the service life of batteries [38], is likely the most significant. According to the adopted Arrhenius type ageing model, given in equation 2, an increase in battery temperature of just 5ºC will reduce battery life by 25%. The impact of temperature becomes more apparent when translated to predicted battery lifetime in km, as shown in Fig. 13. A difference in the average cell surface temperature of only 1°C can result in as much as an 15 thousand km, or 7% decrease in the cell lifetime.

An analysis of the measured temperature data, which included corrections for temperature sensor offset error, determined that temperature during the WLTP ageing cycles was approximately 27.6, 26.8, and 26.6ºC for the 95k, 206k, and 300k cases respectively, as listed in Table 6. The increased temperature causes faster aging as is illustrated in Fig. 2, and offers an explanation for why experimentally observed cell lifetime is less than the lifetime initially

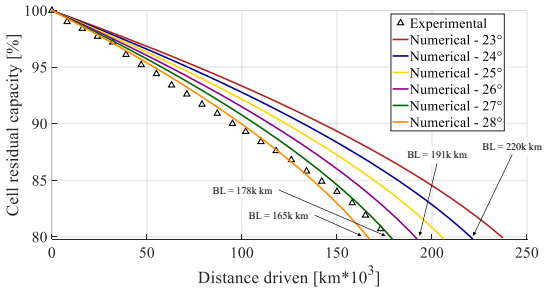

Fig. 13. Sensitivity results for cell ageing as function of surface temperature for the 206k test case.

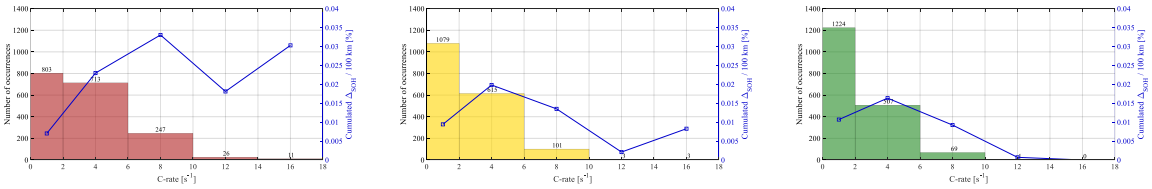

(a) '95k' test case (b) '206k' test case (c) '300k' test case

Fig. 14. Distribution of C-rate values operated by the cells and corresponding predicted cumulative SOH consumption for all test cases.

Table 6

Comparison between numerical predictions and experimental results for lifetime of all tested cells

Test case	Measured Temperature [°C]	Estimated cell lifetime considering measured temperature (WLTP only) [km*10^3]	(WLTP + characterization) [km*10^3]	Experimental cell lifetime [km*10^3]	Difference [%]
'95k'	27.6	78	78	94	-17.0%
'206k'	26.8	183	181	177	+2.3%
'300k'	26.6	279	276	268	+3.0%

forecasted using the numerical ageing model described in Section 2. When utilizing the measured temperatures rather than 25ºC, the predicted lifetime falls by about 20,000 km for each case, as shown in column 3 of Table 6.

The extra cycles for characterization and setting the battery to the 50% SOC can also be considered when calculating the ageing. The 10.5 extra roundtrip cycles, which are performed for each group of 300 WLTP drive cycles, consist of one cycle for the HPPC test, two for the 1C discharge tests, and 15 half cycles for the discharge from 100% to 50% SOC which is performed every 20 WLTP drive cycles. Because the c-rate is so low for these cycles, they only reduce predicted lifetime by at most 3,000 km, as shown in column 4 of Table 6.

In summary, as reported in Table 6, the correlation between numerical predictions and experimental measurements for the values of cell lifetime considerably improves for the 206k and the 300k cases when temperature and the extra cycles are accounted for. The correlation for the 95k test case is made much worse though, with a prediction error of 17% rather than 1.6% as observed with the original modeling. To reduce this error, the shape of the ageing curve, which was extrapolated beyond 10C, will be updated in the following section.

5.2.2 Empirical ageing curve update

Currents above 6C contribute dramatically to battery ageing, as is illustrated in Fig. 14. Because of this, every timestep the battery is providing these high currents have an outsized effect on lifetime. Fig. 14 shows the distribution of current points, and that for the 95k case there are 284 points at 10C or greater, while there are just 107 points for the 206k case and 70 points for the 300k case. The models attribute a substantial amount of ageing to these points, especially for the 95k case, so a small change in how the ageing curve is interpolated between the 6C and 10C experimental points and extrapolated beyond 10C could result in much better alignment between modeled and measured results.

The ageing parameters associated with 8, 12, 14, 16, 18, and 20C current values are therefore updated to achieve better correlation with the experimental results. The new parameters are determined through an iterative calibration procedure which aims to minimize the gap between the updated predicted values of cell lifetime and the corresponding experimental results. The resulting updated ageing curve is overlaid in Fig. 15 with the original curve, and the ageing model parameters which were updated are provided in Table 7. While the changes in the curve appear quite small,

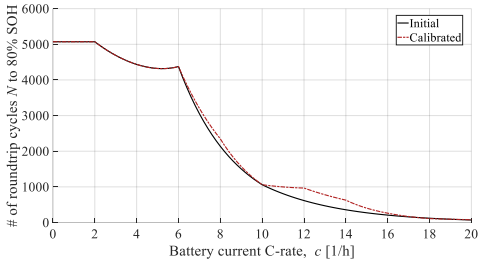

Fig. 15. Update of the number of cell roundtrip cycles as function of the C-rate as a result of the calibration upon obtained experimental data.

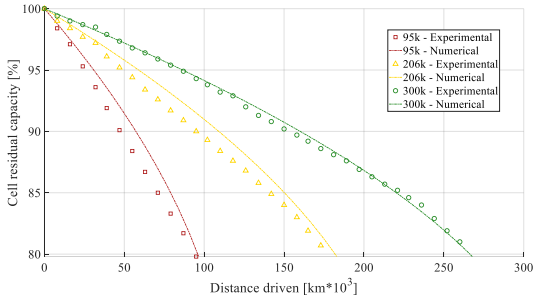

Fig. 16. Correlation between numerical predictions and experimental observations for the cell lifetime of all test cases after the model update.

Table 7

Updated ageing parameters for a A123 26650 cell

Parameter	Value
C-rate index [1/s]	[2 ; 4 ; 6 ; 8 ; 10 ; 12 ; 14 ; 16 ; 18 ; 20]
Empirical pre-exponential factor *B(c)*	[21,681 ; 17,307 ; 12,934 ; 13,512 ; 15,512; 12,099 ; 11,380 ; 13,656 ; 16,342 ; 14,599]

they result in near perfect correlation between measured and updated modeled data as shown in Fig. 16, demonstrating the importance of how the data is extrapolated beyond 10C.

Fig. 16 also demonstrates one other aspect of the model which is not immediately evident, the relation between SOH and cycles is not linear but a power function due to the $Ah_{tp}{}^{z}$ factor in the capacity loss equation (2). The 95k case exhibits a linear ageing trend, while the 300k test case aligns with the nonlinear numerical curve and the 206k case lies between the two tendencies, suggesting the curve shape embedded in the model is only applicable for certain test conditions. Despite this, the updated model parameters result in much better alignment with the experimental data and will therefore be used for the final section of the paper in which performance is investigated for a range of battery pack sizes.

6. Sensitivity analysis based on pack capacity and HEV control optimization goal

This section examines the sensitivity of fuel economy and battery lifetime to the battery pack size and the control goal. To this end, several WLTP drive cycle numerical simulations have been performed for the power-split electrified powertrain layout which is the focus of this study. For the simulations, the battery pack energy capacity is varied from 0.2 to 2.6kWh by adjusting the number of cells in the pack. For each battery pack size two control optimization goals are also considered by varying the coefficient α_{batt} in (9). The first goal, maximizing fuel economy only, is achieved by setting α_{batt} equal to 0, and the second goal, a battery lifetime of 300 thousand km, is achieved by progressively increasing α_{batt} until the desired lifetime is achieved.

Fig. 17 illustrates the numerical results obtained from the sensitivity analysis, reporting fuel consumption and battery lifetime for both control goal cases and for all the considered battery pack sizes. In general, the results show that as the HEV battery pack size increases fuel consumption decreases and battery lifetime improves. Three key points have been identified and highlighted in Fig. 17 for detailed discussion.

Key point A highlights the largest battery pack size considered, 2.6 kWh, where more than 300k km of battery lifetime is achieved when optimizing for fuel economy only. Without consideration of an SOH sensitive EMS, this larger battery pack size would likely be selected by a design engineer. Key point B highlights the smallest battery pack size (1.7 kWh) which can be utilized without a significant increase in fuel consumption for the 300 thousand km battery lifetime case. This 1.7 kWh pack is 35% smaller than the large key point A pack, but results in an increase of fuel consumption of just 1.1%. Likewise, for the

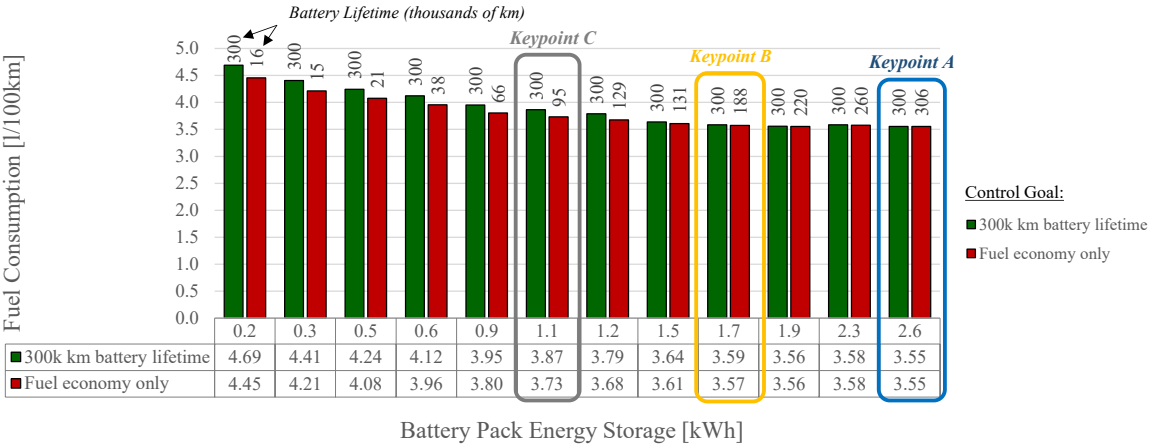

	0.2	0.3	0.5	0.6	0.9	1.1	1.2	1.5	1.7	1.9	2.3	2.6
300k km battery lifetime	4.69	4.41	4.24	4.12	3.95	3.87	3.79	3.64	3.59	3.56	3.58	3.55
Fuel economy only	4.45	4.21	4.08	3.96	3.80	3.73	3.68	3.61	3.57	3.56	3.58	3.55

Fig. 17. Results for fuel economy and battery lifetime depending on the battery pack capacity and the control goal for WLTP.

1.7 kWh pack when controlling for 300 thousand km of battery lifetime rather than for fuel economy only, the predicted battery lifetime increases by 58% and fuel consumption only increases by 0.6%. This suggests that the proposed multi-objective control may allow a considerable downsizing of the HEV battery pack without any substantial deterioration of the fuel economy of the electrified powertrain.

For key point C a much smaller 1.1kWh pack is considered. In this case, to achieve 300 thousand km of battery lifetime fuel consumption is increased by around 3.8% compared to the fuel economy only case, and fuel consumption is increased by 9% compared to key point A. Since the battery pack size of 1.1 kWh is only 42% of the key point A size, this instance demonstrates the potential to maintain battery lifetime while further downsizing of battery pack at the cost of higher fuel consumption. Overall, these examples suggest how design engineers could exploit the illustrated methodology to achieve effective down-sizing of power-split HEV battery packs without excessively reducing fuel economy.

7. Conclusions

This paper deals with the integration of battery lifetime prediction into the optimal energy management of electrified powertrains.

A numerical Ah-based battery ageing model and a power-split HEV powertrain layout are used. Consequently, an optimal multi-objective off-line HEV EMS approach based on DP has been implemented which is capable of optimizing both the fuel economy and the battery lifetime of the HEV. The proposed EMS was used to calculate battery current profiles, assuming a fixed battery temperature of 25°C for battery lifetime cases of 95, 206, and 300 thousand km. An experimental campaign was conducted for the three lifetime cases to validate the numerical battery ageing model, and the model was found to predict lifetime in km with an error ranging from -1.6 to -14.1%. The results achieved with the ageing model were then improved by considering the measured battery temperature (rather than fixed 25°C), by including the characterization tests in the calculation, and by updating how the ageing curve was extrapolated beyond 10C current magnitudes. Thanks to the applied improvements, the overall accuracy of the battery ageing prediction model was considerably improved and now matches the achieved lifetime to within 5%.

Finally, a sensitivity study was performed to assess the impact of the battery pack size and the control optimization goal on the predicted fuel economy and battery lifetime of the retained HEV. The sensitivity results show, thanks to the proposed multi-objective control approach, that for a fixed battery lifetime of 300 thousand km the battery pack can be downsized by 35%, from 2.6 to 1.7kWh, while the fuel consumption increases by only 1.1%.

The proposed methodology is generalized and can be applied to any HEV to allow the battery pack size and vehicle control strategy to be tuned to achieve battery lifetime and vehicle fuel consumption targets. To apply the methodology to other vehicles, an ageing test must first be performed on the batteries of interest and then the aging model presented in section II should be fit to the experimental results. Then the HEV must be modelled with the battery health sensitive EMS, as is done in section III. Finally, an analysis of vehicle fuel consumption and battery lifetime as a function of battery pack size and battery aging cost weighting factor αbatt can be performed, as is done in Fig. 17, to determine the smallest size battery pack which will meet battery lifetime and vehicle fuel consumption goals. A second aging study, as is done in this work to validate the predicted battery lifetime, could also be performed to provide confidence in the model predicted results. The final step, which is beyond the scope of this work, would be to create a real-time version of the proposed control algorithm and to implement it in the HEV.

Related future work could involve improvement of the model fidelity level for both the electrified powertrain and battery ageing, e.g. by accounting for the evolution of the battery temperature over time or by including calendar ageing. Additional testing and correlation activities could also be carried out at the overall battery pack level. Furthermore, rapid near-optimal battery SOH sensitive EMS approaches might be developed to enhance the employment of control optimization techniques in the optimal sizing of electrified powertrains. The reader can refer to [39] for an example of a rapid HEV EMS that could be fostered by integrating the prediction of the HV battery lifetime as a further control goal. Finally, a real-time implementable battery SOH sensitive control approach could be developed and compared to the optimal control approach developed here.

Acknowledgements

This research is supported, in part, thanks to funding from the Natural Sciences and Engineering Research Council of Canada (NSERC), NSERC Industrial Research Chair in Electrified Powertrains, and Canada Research Chair in Transportation Electrification and Smart Mobility. This research work was developed in the framework of the activities of the Interdepartmental Center for Automotive Research and Sustainable Mobility (CARS) at Politecnico di Torino (www.cars.polito.it). The testing was performed at the McMaster Automotive Resource Centre’s Centre for Mechatronics and Hybrid Technologies battery test lab. The authors would like to thank Michael Skells for his help in performing the experimental tests.

References

[1] R.T. Doucette, M.D., McCulloch, “Modeling the prospects of plug-in hybrid electric vehicles to reduce CO2 emissions”, Applied Energy 2011; 88(7): 2315-23.
[2] W. Zhuang, S.L. Eben, X. Zhang, D. Kum, Z. Song, G. Yin, J. Ju, “A survey of powertrain configuration studies on hybrid electric vehicles”, Applied Energy 2020; 262: 114553.
[3] A. Biswas and A. Emadi, "Energy Management Systems for Electrified Powertrains: State-of-the-Art Review and Future Trends", IEEE Transactions on Vehicular Technology 2019; 68(7): 6453-6467.
[4] L. Li, F. Dababneh, J. Zhao, “Cost-effective supply chain for electric vehicle battery remanufacturing”, Applied Energy 2018; 226: 277-86.
[5] P. Tan, H.R. Jiang, X.B. Zhu, L. An, C.Y. Jung, M.C. Wu, L. Shi, W. Shyy, T.S. Zhao, “Advances and challenges in lithium-air batteries”, Applied Energy 2017; 204: 780-806.
[6] F. Gandoman, J. Jaguemont, S. Goutam, R. Gopalakrishnan, Y. Firouz, T. Kalogiannis, N. Omar, J. Van Mierlo, “Concept of reliability and safety assessment of lithium-ion batteries in electric vehicles: Basics, progress, and challenges”, Applied Energy 2019; 251: 1-17.
[7] C. Yang , S. Du, L. Li, S. You, Y. Yang, Y. Zhao, “Adaptive real-time optimal energy management strategy based on equivalent factors optimization for plug-in hybrid electric vehicle”, Applied Energy 2017; 203: 883-896.
[8] Y. Yang, X. Hu, H. Pei, Z. Peng, “Comparison of power-split and parallel hybrid powertrain architectures with a single electric machine: Dynamic programming approach”, Applied Energy 2016; 168: 683-690.
[9] C. Hou, M. Ouyang, L. Xu, H. Wang, “Approximate Pontryagin’s minimum principle applied to the energy management of plug-in hybrid electric vehicles”, Applied Energy 2014; 115: 174-89.
[10] S. Ebbesen, P. Elbert and L. Guzzella, "Battery State-of-Health Perceptive Energy Management for Hybrid Electric Vehicles", IEEE Transactions on Vehicular Technology 2012; 61(7): 2893-2900.
[11] L. Tang, G. Rizzoni and S. Onori, "Energy Management Strategy for HEVs Including Battery Life Optimization", IEEE Transactions on Transportation Electrification 2015; 1(3): 211-222.

[12] S. Zhang, X. Hu, S. Xie, Z. Song, L. Hu, C. Hou, “Adaptively coordinated optimization of battery aging and energy management in plug-in hybrid electric buses”, Applied Energy 2019; 256: 1-15.b

[13] S. Xie, X. Hu, Q. Zhang, X. Lin, B. Mu, H. Ji, “Aging-aware co-optimization of battery size, depth of discharge, and energy management for plug-in hybrid electric vehicles”, Journal of Power Sources 2020; 450: 1-11.

[14] M. Cheng and B. Chen, "Nonlinear Model Predictive Control of a Power-Split Hybrid Electric Vehicle With Consideration of Battery Aging", ASME. J. Dyn. Sys., Meas., Control 2019; 141(8): 081008.

[15] N. Guo, X. Zhang, Y. Zou, L. Guo, G. Du, “Real-time predictive energy management of plug-in hybrid electric vehicles for coordination of fuel economy and battery degradation”, Energy 2021; 214: 119070.

[16] L. De Pascali, F. Biral and S. Onori, "Aging-Aware Optimal Energy Management Control for a Parallel Hybrid Vehicle Based on Electrochemical-Degradation Dynamics", IEEE Transactions on Vehicular Technology 2020; 69(10): 10868-10878.

[17] S. Xie, S, Qi, K. Lang, X. Tang, X. Lin, “Coordinated management of connected plug-in hybrid electric buses for energy saving, inter-vehicle safety, and battery health”, Applied Energy 2020, no. 115028.

[18] R. Du, X. Hu, S. Xie, L. Hu, Z. Zhang, X. Lin, “Battery aging- and temperature-aware predictive energy management for hybrid electric vehicles”, Journal of Power Sources 2020; 473: 228568.

[19] S. J. Moura, J. L. Stein and H. K. Fathy, "Battery-Health Conscious Power Management in Plug-In Hybrid Electric Vehicles via Electrochemical Modeling and Stochastic Control", IEEE Transactions on Control Systems Technology 2013; 21(3): 679-694.

[20] C. Patil, P. Naghshtabrizi, R. Verma, Zhijun Tang, K. Smith and Ying Shi, "Optimal battery utilization over lifetime for parallel hybrid electric vehicle to maximize fuel economy," 2016 American Control Conference (ACC), Boston, MA, 2016, pp. 1524-1529.

[21] P. J. Kollmeyer, T. M. Jahns, “Ageing and performance comparison of absorbed glass matte, enhanced flooded, PbC, NiZn, and LiFePO4 12V start stop vehicle batteries”, Journal of Power Sources 2019; 441: 227139.

[22] Z. Liu, A. Ivanco, S. Onori, “Aging characterization and modeling of nickel-manganese-cobalt lithiumion batteries for 48V mild hybrid electric vehicle applications”, Journal of Energy Storage 2019; 21: 519-527.

[23] D.U. Sauer, H. Wenzl, “Comparison of different approaches for lifetime prediction of electrochemical systems—Using lead-acid batteries as example”, Journal of Power Sources 2008; 176(2): 534-546.

[24] J. Zhua, M. Knappa, M. S. Dewi Darmab, Q. Fangc, X. Wangc, H. Daic, X. Weic, H. Ehrenberga, “An improved electro-thermal battery model complemented by current dependent parameters for vehicular low temperature application”, Applied Energy 2019; 248: 149-161.

[25] S. Han, S. Han, H. Aki, “A practical battery wear model for electric vehicle charging applications”, Applied Energy 2014; 113: 1100-1108.

[26] I. Bloom, B. W. Cole, J. J. Sohn, S. A. Jones, E. G. Polzin, V. S. Battaglia, G. L. Henriksen, C. Motloch, R. Richardson, T. Unkelhaeuser, D. Ingersoll, and H. L. Case, “An accelerated calendar and cycle life study of Li-ion cells”, Journal Power Sources 2001; 101(2): 238–247.

[27] P. G. Anselma, P. Kollmeyer, G. Belingardi and A. Emadi, "Multi-Objective Hybrid Electric Vehicle Control for Maximizing Fuel Economy and Battery Lifetime," *2020 IEEE Transportation Electrification Conference & Expo (ITEC)*, Chicago, IL, USA, 2020, pp. 1-6

[28] J. Wang, P. Liu, J. Hicks-Garner, E. Sherman, S. Soukiazian, M. Verbrugge, H. Tataria, J. Musser, and P. Finamore, “Cycle-life model for graphite- LiFePO4 cells”, Journal Power Sources 2011; 196(8): 3942– 3948.

[29] P. G. Anselma, Y. Huo, J. Roeleveld, G. Belingardi and A. Emadi, "Slope-Weighted Energy-Based Rapid Control Analysis for Hybrid Electric Vehicles," in IEEE Transactions on Vehicular Technology, vol. 68, no. 5, pp. 4458-4466, May 2019.

[30] R. H. Staunton, C. W. Ayers, J. N. Chiasson, B. A. Burress and L. D. Marlino, “Evaluation of 2004 Toyota Prius hybrid electric drive system”, *Oak Ridge National Lab. (ORNL),* 2006.

[31] A123 systems, "Nanophosphate® High Power LithiumIon Cell ANR26650M1-B", [online] https://www.batteryspace.com/prod-specs/6610.pdf (accessed 10 June 2020).

[32] Meisel, J., "An Analytic Foundation for the Toyota Prius THS-II Powertrain with a Comparison to a Strong Parallel Hybrid-Electric Powertrain," SAE Technical Paper 2006-01-0666, 2006.

[33] J. Lempert, B. Vadala, K. Arshad-Aliy, J. Roeleveld and A. Emadi, "Practical Considerations for the Implementation of Dynamic Programming for HEV Powertrains," 2018 IEEE Transportation Electrification Conference and Expo (ITEC), Long Beach, CA, 2018, pp. 755-760.

[34] O. Sundstrom and L. Guzzella, "A generic dynamic programming Matlab function," 2009 IEEE Control Applications, (CCA) & Intelligent Control, (ISIC), St. Petersburg, 2009, pp. 1625-30.

[35] Engbroks, L., Knappe, P., Goerke, D., Schmiedler, S., Goedecke, T. and Geringer, B., "Energetic Costs of ICE Starts in (P)HEV - Experimental Evaluation and Its Influence on Optimization Based Energy Management Strategies," SAE Technical Paper 2019-24-0203, 2019.

[36] US Department of Energy, "eGallon: Compare the costs of driving with electricity", [online] https://www.energy.gov/maps/egallon (accessed 11 June 2020).

[37] L. Serrao, S. Onori, A. Sciarretta, Y. Guezennec and G. Rizzoni, "Optimal energy management of hybrid electric vehicles including battery ageing," Proceedings of the 2011 American Control Conference, San Francisco, CA, 2011, pp. 2125-2130.

[38] M.l Woodya, M. Arbabzadeha, G. M. Lewisa, G. A. Keoleiana, A. Stefanopoulou , “Strategies to limit degradation and maximize Li-ion battery service lifetime - Critical review and guidance for stakeholders”, Journal of Energy Storage 2020; 28: 101231.

20 P.G. Anselma, P. Kollmeyer, J. Lempert, Z. Zhao, G. Belingardi, A. Emadi, “Battery state-of-health sensitive energy management of hybrid electric vehicles: Lifetime prediction and ageing experimental validation”, Applied Energy, vol. 285, no. 116440, 2021.

[39] P.G. Anselma, A. Biswas, G. Belingardi, A. Emadi, “Rapid assessment of the fuel economy capability of parallel and series-parallel hybrid electric vehicles”, Applied Energy 2020; 275: 115319.